Electronic consequences of random layer thickness fluctuations in AlAs/GaAs superlattices

Kurt A. Mäder, Lin-Wang Wang, and Alex Zunger

Citation:

Electronic consequences of random layer-thickness fluctuations in (isoelectronic AlAs/GaAs superlattices

[redacted]

(Received 12 June 1995; accepted for publication 24 August 1995)

We study the effects of a few types of atomic disorder on the electronic and optical properties of AlAs/GaAs (001) and (111) superlattices: (i) atomic intermixing across the interfaces; (ii) replacing [redacted] doping); and (iii) random layer-thickness fluctuations in superlattices (SL). Type (i) is an example of lateral disorder, while types (ii) and (iii) are examples of vertical disorder. Using three-dimensional empirical pseudopotential theory and a plane-wave basis, we calculate the band gaps, electronic wave functions, and optical matrix elements for systems containing up to 2000 [redacted] from the band edges in vertically disordered SLs. Our main findings are: (i) Chemical intermixing across the interface can significantly shift the SL energy levels and even change the identity (e.g., symmetry) of the conduction-band minimum in AlAs/GaAs SLs; (ii) any amount of thickness fluctuations in SLs leads to band-edge wave-function localization; (iii) these fluctuation-induced bound states will emit photons at energies below the "intrinsic" absorption edge (red shift of [redacted] AlAs/GaAs SLs with monolayer thickness fluctuations have a direct band gap, while the ideal (001) superlattices are indirect for $n<4$; (vi) there is no mobility edge for vertical transport in a disordered [redacted] intentionally disordered SLs [A. Sasaki, J. Cryst. Growth **115**, 490 (1991)], explaining the strong intensity and large red shift of the photoluminescence in the latter system. We provide predictions [redacted] © *1995 American Institute of Physics.*

I. INTRODUCTION

Experimental and theoretical research on semiconductor superlattices (SL) has, for a long time, focused on ideal, [redacted] layer thicknesses n and m of the two materials A and G, respectively, while theorists calculated the electronic structure of these ideal structures by applying periodic boundary [redacted] flicts between experiment (e.g., spectroscopy) and theory (e.g., envelope function $k\cdot p$) are often settled by adjusting some of the theoretical fitting parameters (band offsets, Luttinger parameters, layer thicknesses), thus restoring agreement with experiment. In recent years, attention has shifted somewhat away from ideal to nonideal SLs in two ways: First, with the advent of more sensitive characterization techniques, it has become evident that not only are semiconductor interfaces almost never ideal, but that this unintentional disorder in real samples has discernible spectroscopic and transport consequences[1–10] that should be taken into account by theory. Second, *intentionally* disordered SLs have been proposed[11,12] and grown,[13–15] revealing very interesting disorder-induced effects on the electronic, transport, and optical properties.

Disorder in a SL can be broadly classified in two catego-

[redacted]

(i) Lateral disorder in the (x,y) substrate plane[1–5] [Fig. 1(a)], and

(ii) Vertical disorder along the SL growth direction (z) in [redacted][6–10] [Fig. 1(b)].

Lateral disorder occurs in the form of chemically intermixed interfaces,[1–3] steps,[4] or islands[5] protruding from material A into G, and vice versa. The translational symmetry of the SL is broken in the (x,y) plane. When averaging over [redacted] der produces a graded, continuous composition profile along the z axis. Thus, if all of the interfaces in a laterally disordered SL are equivalent, the one-dimensional (1D) periodicity along the growth direction is preserved on average.

Vertical disorder, on the other hand, is characterized by a discrete composition profile along z. Here the interfaces are reasonably flat in the (x,y) plane, but the A and G layer thicknesses fluctuate around their nominal values. The translational symmetry of the SL along z is broken, and the dis-

[a]Present address: Centre Européen de Calcul Atomique et Moléculaire, Ecole Normale Supérieure, 46, Allée d'Italie, 69364 Lyon Cedex 07, France; Electronic mail: mader@cecam.fr

 0021-8979/95/78(11)/6639/19/$6.00

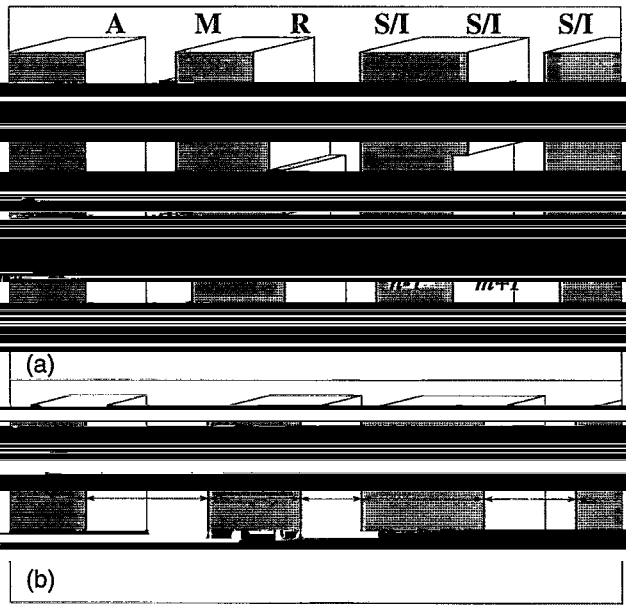

tical disorder along the superlattice orientation. The interface structures sketched in cross section in (a) are atomically abrupt (A), "microrough" or intermixed (M), rough (R), and stepped or islanded (S/I). (The letters a, m, r, s, i can be distinguished in cross section.) In (b) the layer thicknesses fluctuate, assuming integer values $n, n', n'', \ldots$ monolayers, while the indi-

order is "quasi one dimensional" (which does not mean, however, that the Schrödinger equation can be separated into a 1D disordered and a 2D ordered system).

Unintentional disorder is likely to consist of both types of disorder.[16,17] The experimentally observable types of disorder depend critically on the coherence length of the experimental probe (x-ray diffraction, electron microscopy, Raman scattering, etc.). Lateral disorder, for example, has been shown to exhibit a rather complex "roughness spectrum," scales.[4,18] If the roughness spectrum is bimodal[18] having ...ge scales and the coherence length of the probe is much large roughness scale, then the probe will "see" an ensemble

these terms, because they exhibited a set of rather sharp

in quantum wells of various thicknesses.[7,10,19] If the probe involves excitation of a valence hole or a conduction electron in a cubic semiconductor, its response will predominantly reflect the small length scales (of the order of a few lattice constants). Therefore, if lateral imperfections occur in the form of atomic intermixing, the effect on the SL band structure is noticeable predominantly in short-period SLs, but less significant in long-period SLs or multiple quantum wells (where the electrons "see" mostly bulk, and little interface).

If, on the other hand, lateral imperfections consist of large islands, or well-separated steps, the system resembles, in terms of the electronic structure, a SL with vertical thickness

the interfaces labeled "S/I" in Fig. 1(a)].

use a random number generator to establish a particular

and great care is taken to assess the effects of any possible lateral imperfections that could interfere with the wanted ef-

largely concentrated on strictly one-dimensional one-band models, such as Kronig–Penney models using the effective mass approximation (EMA), or one-dimensional tight-binding models.[11,25,26] Within 1D models, lateral imperfections are simulated by graded, sinusoidal potential profiles corresponding to composition profiles averaged in the (x,y)

in the form of mathematically 1D models, if one is willing to ignore the truly 3D crystal structure of a SL. A vast literature exists on localization in 1D disordered systems,[29,30] and

rule exist for *deterministic* forms of 1D disorder, some of which have been realized experimentally in 3D SLs, e.g., AlAs/GaAs Fibonacci SLs.[13,35,36]

Studies on nonideal SLs using three-dimensional band-

unit cells are required to simulate the absence of periodicity

intermixing in $(AlAs)_1/(GaAs)_1$ (001) SLs has been studied using the local-density approximation (LDA) by considering reconstructed interfacial unit cells with atomic swaps across the interface.[37] 2D tight-binding calculations on disordered SLs were described by Wang *et al.*, and on quasiperiodic SLs by Hirose and co-workers[36] and by Kumar and

In this article we present 2D electronic structure calcu-

layer thicknesses (vertical disorder) and with interfacial

and unintentional thickness fluctuations. A 3D description of the energy bands is particularly important for short-period

originating from different points in the Brillouin zone. Dis-

erties relative to their ordered counterparts with the same composition:

(a) strong and initially fast decaying (lifetime $\tau = 0.25$ ns at $T = 77$ K) photoluminescence (PL) intensity [43] even

though the equivalent ordered $(AlAs)_2/(GaAs)_2$ SL has an indirect band gap and thus emits both weakly and slowly;

(b) A large red shift (~60 meV) of the PL peak[44,45] with respect to the equivalent *o*-SL;

(c) An order-of-magnitude slower rate of reduction of the PL intensity with temperature,[46] and

(d) Nonexponential PL intensity decay at long times[45]

These unusual properties of *d*-SLs appear very attractive for

on these two types of intentionally disordered SLs has been published in Ref. 47.

(i) The lack of translational symmetry requires the use of unit cells with a macroscopic length $N \approx 1000$ mono-

($Na \approx 500$ nm, where a is the monolayer thickness);

over, occur on a microscopic length scale of about 0.1 nm.

While it is possible to rescale the microscopic length scale by replacing the periodic atomic potential by an external, rectangular potential, this approach fails to describe impor-

microscopic pseudopotential description of the electron structure to a macroscopic length scale necessitated by the absence of translational symmetry. We use fixed (screened)

band structures, effective masses, deformation potentials, band offsets, and energy levels in superlattices.[48] This is also called the empirical pseudopotential method (EPM) in the following. The wave functions are expanded in a basis of

"folded-spectrum" method,[49] where eigenstates are obtained

gap), without having to solve for any of the lower-lying eigenstates first, thus circumventing the need for orthogonalization. The effort scales linearly with the number of atoms, allowing us to use the realistic, three-dimensional pseudopotentials, and to solve the Schrodinger equation in a highly flexible plane-wave basis even for $N=1000$ ML. Following these accurate pseudopotential calculations, we also performed EMA calculations

(i) to check the validity of the effective mass method, and

(ii) to obtain some statistical properties of the electronic states away from the band edge.

The remainder of the article is organized as follows. In

electronic Hamiltonians are discussed in Sec. III. In Sec. IV

pseudopotential and 1D effective mass results on disordered SLs are presented. Conclusions and a summary are presented in Sec. V.

II. MODELING THE STRUCTURE OF SUPERLATTICES WITH RANDOM LAYER-THICKNESS FLUCTUATIONS

An ordered ideal superlattice is characterized by a unit cell A_nG_m that is repeated periodically, and which contains n monolayers of material A and m monolayers of material

however, instead of the periodic sequence $n,m,n,m,...$ we

[see Fig. 1(b)]. The SL is thus no longer described by the small, $n+m$ atoms unit cell A_n/G_m. Instead, we use a large unit cell that can be described by (normalized) distribution

however, be easily relaxed by allowing $p_\alpha(0)>0$. For example, $p_G(0)>0$ means "skip a layer of material G" with probability $p_G(0)$.] By requiring the two materials A and G to alternate, one considers in effect the joint distribution function $P(A_nG_m)$ of one-dimensional "molecules" A_nG_m,

Sasaki *et al.*[15] chose this type of random sequence, with

The form of Eq. (1) is also expected in SLs with unintentional random thickness fluctuations, if these fluctuations do not depend on the material deposition sequence (i.e., if there

growing A-on-G).

Modifications of Eq. (1) have also been considered in intentionally disordered SLs. Chomette *et al.*[14] fixed the thickness of the AlAs segments to a constant n_0, hence, $P(A_nG_m)=p_G(m)\,\delta(n-n_0)$, (where $n_0 \approx 10$), and $p_G(m)$ was chosen to be a discrete Gaussian distribution around a mean thickness $\langle m \rangle \approx 10$ ML. Arent *et al.*[45] on the other hand, fixed the length $M=n+m$ of each "molecule" using $P(A_nG_{M-n})=p(n)$, where the distribution $p(n)$ was chosen to be the same as that used by Sasaki *et al.*[15] In this approach $p_A(n)$ and $p_G(m)$ are completely correlated, since knowledge of one completely specifies the other. Therefore, in contrast to Sasaki *et al.*'s *d*-SL, Arent *et al.*'s variation corresponds to partially ordered SLs (po-SL), retaining long-range order.

SL direction is conveniently measured in terms of the

it, one assigns a pseudospin variable S_i of value $+1$ (-1) if

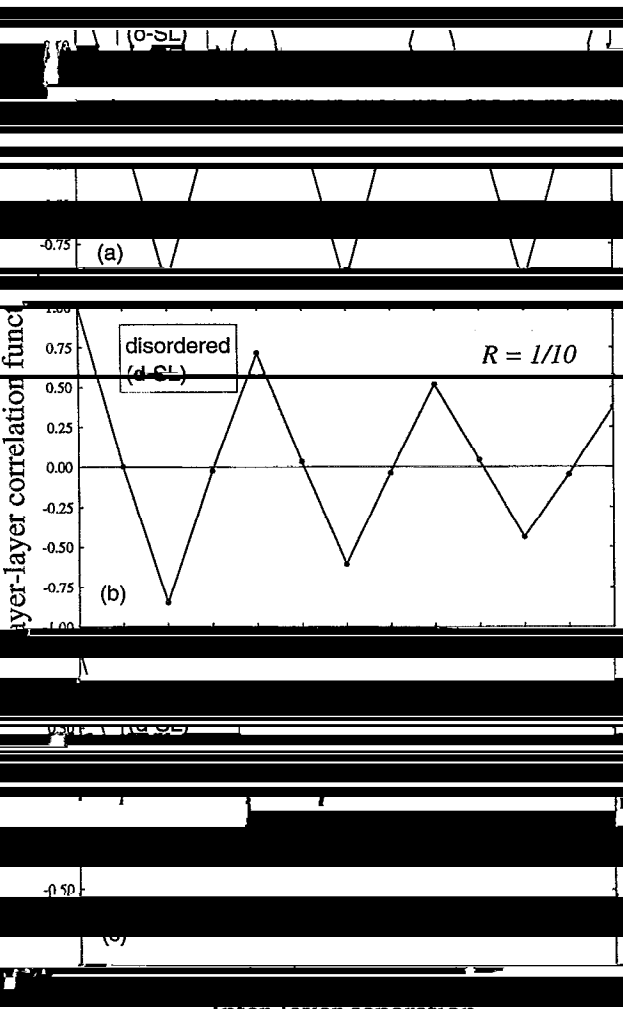

FIG. 2. Layer–layer correlation function $\langle \Pi_2(j) \rangle$ [Eq. (2)] of (a) an ordered $(A)_2/(G)_2$ superlattice (o-SL), (b) a disordered superlattice (d-SL) with a small degree $R=1/10$ of thickness fluctuations [Eq. (3)], and (c) a d-SL with maximum disorder $R=1$.

monolayer i is occupied by material $A(G)$. The pair-correlation function for two monolayers separated by dis-

where sum runs over the N monolayers of a particular realization of the SL, and the angular brackets denote a configurational average. In an ordered A_n/G_m SL we have in Eq. (2) $N=n+m$ and $\langle \Pi_2(j) \rangle$ is a periodic function with periodicity $n+m$. This is illustrated in Fig. 2(a) for an A_2/G_2 o-SL, whose $\langle \Pi_2(j) \rangle$ is seen to be a (discrete) periodic function with amplitude unity and periodicity $N=n+m=4$. For a disordered SL, however, we must perform the configurational average in Eq. (2), or equivalently consider the limit

$[p(2)=\frac{5}{6}$ and $p(1)=p(3)=\frac{1}{12}]$, i.e., for a d-SL with average

ure 2(c) shows the same quantity for a large degree of dis-

In the special case of monolayer thickness fluctuations $n'=n\pm1$ around a given (ideal) layer thickness n we can

tive frequency of the respective thickness fluctuations $n+1$

$$R=\frac{p(n+1)}{p(n)}=\frac{p(n-1)}{p(n)}. \tag{3}$$

Because the distribution $p(n')$ is normalized, we can write $p(n)=1/(1+2R)$ and $p(n\pm1)=R/(1+2R)$. For the ideal, ordered $n\times n$ superlattice $R=0$, and $p(n')=\delta(n'-n)$, whereas for a d-SL with $R=1$ all three layer thicknesses $\{n-1,n,n+1\}$ occur with equal probability $p=\frac{1}{3}$. The minimum value of R that can be reached in a SL of finite length N corresponds to a single "chain mutation," (a single

refer to this limiting case by the notation $R\to0$ (distinct from

(i.e., one out of ten layers has a thickness of $n+1$ or $n-1$ ML, respectively). Indeed, the correlation function decays

Fig. 2(c), and the "ideal" periodicity of 4 ML is still clearly

The one-dimensional Fourier transform of the real-space correlation functions of Eq. (2) equals $|S(k_\parallel)|^2$, where $k_\parallel$ is a wave vector along the SL direction. The form factor $|S(k_\parallel)|^2$ is proportional to the diffuse scattering intensity of a kinematic scattering experiment at zero temperature. Figure 3(a) shows $|S(k_\parallel)|^2$ of the ordered SL with correlation function $\langle \Pi_2(j) \rangle$ depicted in Fig. 2(a), for $k_\parallel$ lying in the first Brillouin zone of the empty linear chain. Clearly, the "diffuse scattering" of the o-SL consists of the new Bragg, or satellite peaks

because of the particular unit cell choice $n=m=2$.) $|S(k_\parallel)|$

to true diffuse scattering throughout the 1D Brillouin zone. The average periodicity $\langle n \rangle+\langle m \rangle=4$ still leaves fingerprints at the peak positions of the o-SL. (In the case $R=1$, there is also a maximum at the previously forbidden wave vector $k_\parallel=\frac{1}{2}$.)

In the special case of a partially ordered SL,[45] the layer-layer correlation function $\langle \Pi_2(j) \rangle$ is periodic, but its amplitude is smaller than that of the ideal o-SL. Figure 4 shows $\langle \Pi_2(j) \rangle$ for po-SLs with $\langle n \rangle=2$, $R=\frac{1}{10}$, and $R=1$ exhibiting

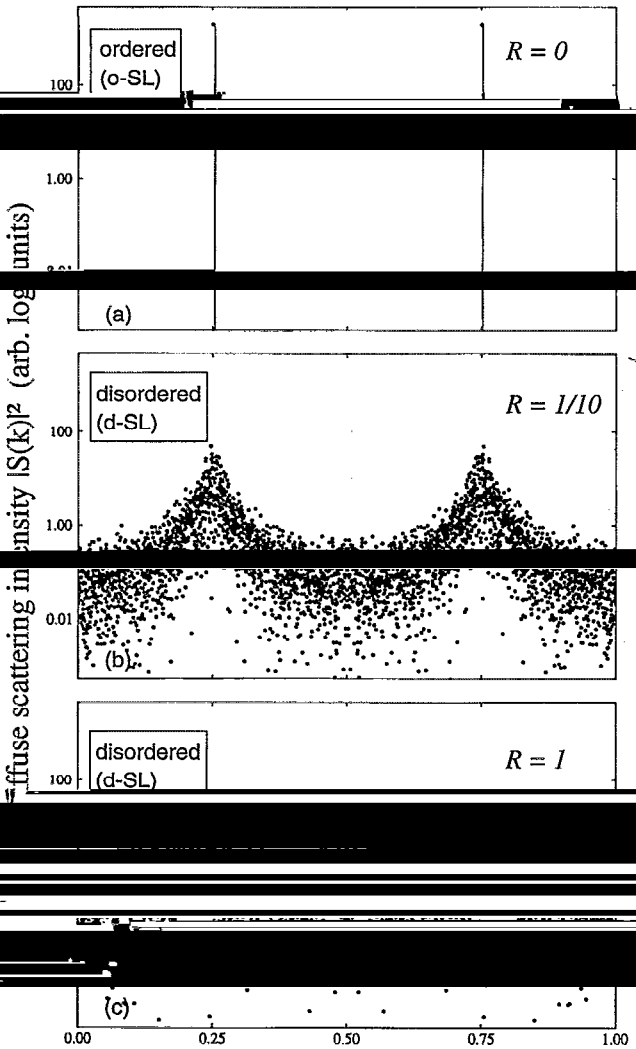

FIG. 3. The diffuse scattering intensities $|S(k_\parallel)|^2$ of the d-SLs shown in Figs. 2(a), 2(b), and 2(c), respectively.

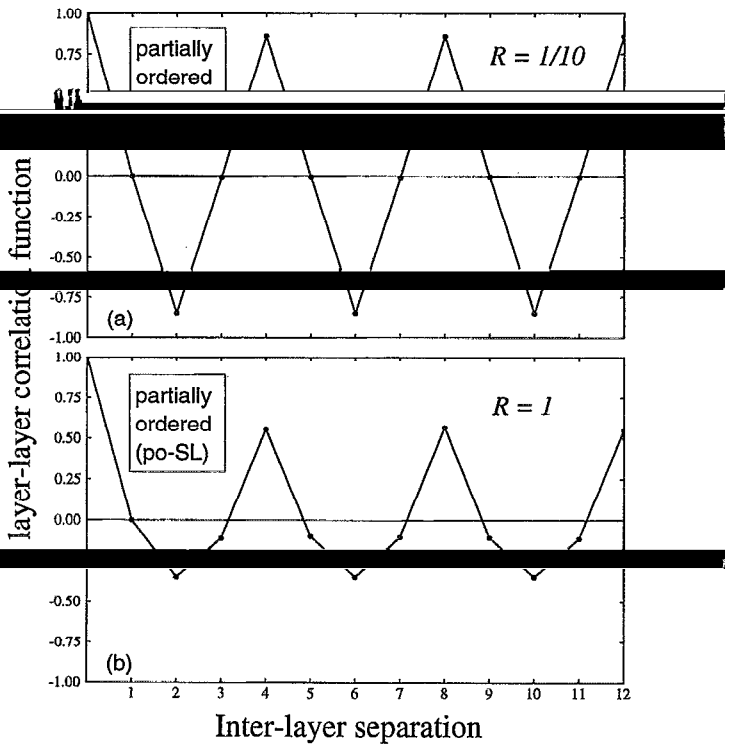

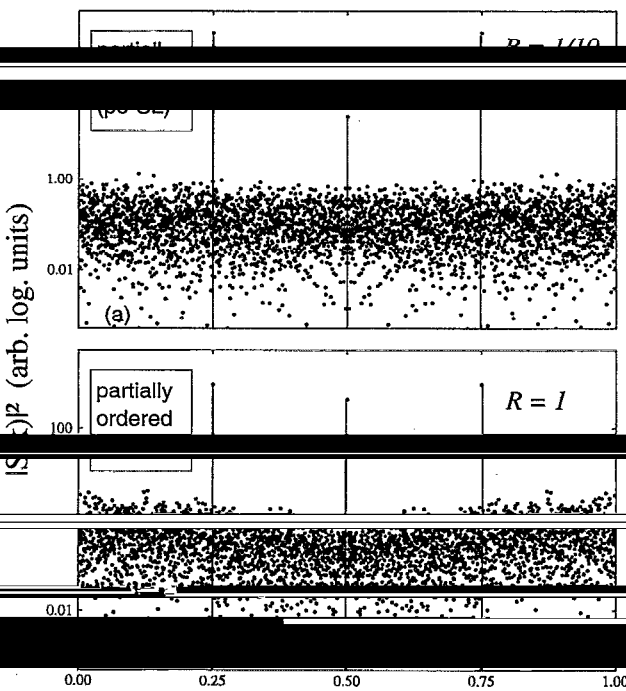

Figs. 4(a) and 4(b), respectively.

coexistence of rather strong peaks at the o-SL peak positions (marked by vertical impulses) and a diffuse background of comparable amplitude than in a d-SL (Fig. 3).

The appearance of diffuse scattering intensity in a d-SL is in fact a manifestation of the relaxation of the $k_\parallel$ selection rule due to the breaking of translational symmetry in the d-SL. We see in the following sections that the relaxation of the $k_\parallel$ selection rule has a profound effect also on the electronic structure of disordered superlattices.

III. ELECTRONIC STRUCTURE CALCULATIONS

A. Three-dimensional pseudopotential representation

1. The pseudopotential and the basis set

Given the crystal structure of an ordered or disordered SL

where $V(x,y,z)$ is the three-dimensional screened local pseudopotential,

$$V(\mathbf{r})=\sum_{\alpha}\sum_{R} v_{\alpha}(|\mathbf{r}-\tau_{\alpha}-\mathbf{R}_n|), \tag{5}$$

cells n of the screened atomic pseudopotentials $v_\alpha(r)$. We have recently parameterized $v_\alpha(r)$ for α=Ga, Al, and As, so as to fit the experimentally measured band structures of bulk

$(GaAs)_n/(AlAs)_n$ superlattices. A detailed comparison of the bulk properties calculated with these empirical pseudopotentials and the experimentally observed properties is given in Ref. 48. An important aspect of this pseudopotential is that the arsenic potential depends on the identity of its four nearest neighbors, i.e., the number of Al and Ga atoms around it. This introduces important interfacial effects: the potential $V(\mathbf{r})$ changes from GaAs-like to a mixed GaAlAs type at the interface and finally to AlAs-like. Thus, while $V(\mathbf{r})$ is not calculated self-consistently, it was constrained to correctly describe LDA-calculated superlattices via introduction of such interfacial effects. This feature distinguishes our empirical pseudopotential calculations from other calculations of superlattices (see review of other calculations in Ref. 48).

Equation (4) is solved by expanding $\psi_j(\mathbf{r},\mathbf{k})$ in plane

$$\psi_j(\mathbf{r},\mathbf{k})=\sum_{G}^{G_{\max}} A_j(\mathbf{k},\mathbf{G})e^{i(\mathbf{k}+\mathbf{G})\cdot\mathbf{r}}, \tag{6}$$

matrix elements of $V(\mathbf{r})$ in the basis set of Eq. (6) are calculated by a Fourier transform, with no approximation except truncation: The basis set (6) is truncated at some maximum value of $G_{\max}$=2.24 a.u. (resulting in about 30 plane waves per atom in GaAs/AlAs systems) determined in the construc-

3D problem. Note also that no use is made of effective-mass, $k\cdot p$, or envelope-function approximations here.

2. Solving the Schrödinger equation

Substitution of the plane-wave expansion of Eq. (6) into the Schrödinger equation Eq. (4) results in a matrix (secular) equation whose dimension is $N_G\times N_G$, where N_G is the number of plane waves entering Eq. (6). In practice, this

$N\sim 1000$ ML. Standard techniques for solving Schrödinger's equation require orthogonalization of each state to all other states, thus leading to an N_G^3 scaling of the effort involved.

energy levels. It was recently shown[49] that one could replace Eq. (4) by

$$[-\tfrac{1}{2}\nabla^2+V(\mathbf{r})-\epsilon_{\text{ref}}]^2\psi_j(\mathbf{r},\mathbf{k})=(\epsilon_j-\epsilon_{\text{ref}})^2\psi_j(\mathbf{r},\mathbf{k}), \tag{7}$$

where ϵ_{ref} is an arbitrary "pointer" and $\{\epsilon_j,\psi_j\}$ are identical

(7) corresponds, however, to the eigenvalue closest to ϵ_{ref}. Thus, by placing the "pointer" ϵ_{ref} inside the band-gap region, one is guaranteed to find the valence-band maximum

problems can be solved readily. Reference 49 provides technical details on the preconditioned conjugate-gradient algorithm used to solve Eq. (7). The solutions of Eq. (7) obtained this way are *exact*, equalling those of Eq. (4).

B. One-dimensional envelope-function model

In this subsection, we describe the effective-mass model used in addition to the pseudopotential method to calculate the electronic structure of the disordered SL. By using the effective mass model, we are able to find the eigenstates even far away from the band edge and obtain statistical properties of the states by calculating many different random se-

Using the Kronig–Penney effective mass model, the three-dimensional problem of Eq. (4) is reduced to the one-dimensional problem

$$\left(-\frac{1}{2}\frac{d}{dz}\frac{1}{m^*(z)}\frac{d}{dz}+V_{\text{ext}}(z)\right)\phi_i(z)=\epsilon_i\phi_i(z). \tag{8}$$

Here $m^*(z)$ is the effective mass, $V_{\text{ext}}(z)$ is the external potential [to be distinguished from the microscopic atomic potential of Eqs. (4) and (5)] and $\phi_i(z)$ is the envelope func-

effective mass $m^*(z)$. Like in the empirical pseudopotential calculation, we assume periodic boundary conditions for the supercell. This is equivalent to connecting the left-hand end of the SL with its right-hand end. Written in the form of Eq. (8), we imply that the boundary condition at the GaAs/AlAs interface is the continuity of $\phi_i(z)$ and $m^*(z)^{-1}(d/dz)\phi_i(z)$. More explicitly, we have

$$\left(m^{*-1}\frac{d\phi(z)}{dz}\right)_{\text{GaAs-IF}}=\left(m^{*-1}\frac{d\phi(z)}{dz}\right)_{\text{AlAs-IF}}, \tag{9}$$

layer both m^* and V_{ext} are constants. Let us denote by l the layer index ($l=1,\ldots N$, running from left- to right-hand side). Then, m_l^*, V_l, and the layer length d_l specify the physical

(where z_l is the left-hand-side position of the lth layer), then from Eq. (8) A_{l+1} is given by

For $E \geqslant V_l$ and $k = \sqrt{2m_l^*(E-V_l)}$, we have

$$M_l(E)=\begin{pmatrix} \cos(kd_l) & \sin(kd_l)/k \\ -km_{l+1}^* \sin(kd_l)/m_l^* & m_{l+1}^* \cos(kd_l)/m_l^* \end{pmatrix}, \tag{12}$$

while for $E<V_l$ and $k = \sqrt{2m_l^*(V_l-E)}$ we have

$$M_l(E)=\begin{pmatrix} \cosh(kd_l) & \sinh(kd_l)/k \\ \cdots & \cdots \end{pmatrix}. \tag{13}$$

To solve for an eigenstate $\phi_i(z)$ and an eigenvalue ϵ_i of

$$A_{N+1}=\left(\prod_{l=1}^{N} M_l(E)\right)A_1=A_1. \tag{14}$$

The ith solution of E yields ϵ_i whereas the ith solution of A_i yields $\phi_i(z)$.

and scan $d(E)$ within the interesting range of E. A change of sign in $d(E)$ when E increases indicates a solution. Then Newton's iteration method is used to find the exact E value which yields the zero of $d(E)$. However, for the d-SL, when E is close to the band edge, this procedure is numerically unstable for large N due to the typical exponential growth of $\Pi_{l=1}^{N} M_l(E)$ as a function of N. In this case, we need another procedure to find localized states. We start with $A_1=[0,1]$ and scan $A_{N+1}(E)=[a(E),b(E)]$ as a function of E. Then if $\phi_i(z)$ belonging to this E has large amplitude near $l=1$ or

culated by shifting the starting (the ending) position from $l=1$ ($l=N$) to another point, so that this localized state is in the middle of the starting and ending points.

By switching between the above two procedures, we can reliably calculate all the states of a one-dimensional system for almost arbitrarily large N.

To solve the 1D problem we need to determine the external potential V_{ext} (i.e., band lineups) and effective masses,

are given in Fig. 6. Since the AlAs X_{1c} state is near the CBM, for small period superlattice, the X valley derived electron state could be important. For large period superlattices, the absolute CBM is the GaAs Γ_{1c} state, thus Γ valley derived electron states are important. Thus, for electron

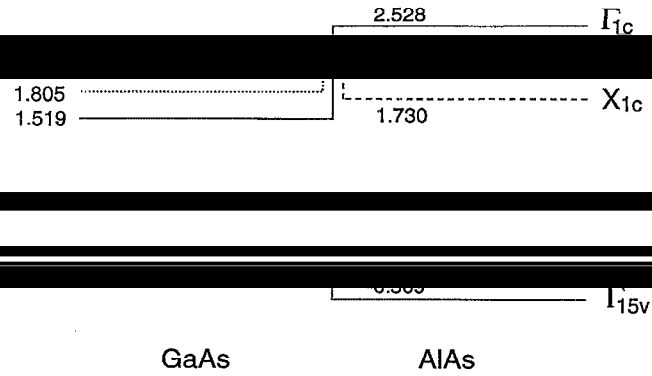

FIG. 6. Band offsets (eV) used for the GaAs/AlAs interface. These band edge energies yield their corresponding potential $V(z)$ in the effective-mass calculation of Eq. (8).

states, we calculate states derived from Γ and X valleys. The L valley derived states is also calculated in some cases to compare with the pseudopotential results. For holes we only

pseudopotential for the (001) and (111) directions using $m^* \approx \Delta k^2/2\Delta E$ are shown in Table I. Using the band offsets of Fig. 6 and the masses given in Table I, we can calculate the electronic structure of superlattices using the EMA of Eq. (8).

In this section, we discuss the following cases:

(a) The ideal ordered superlattice of period n. Here $R \equiv 0$ and $p(n')=\delta(n'-n)$. This will establish the electronic structure of our "unperturbed system" (Sec. IV A);

TABLE I. EPM effective masses (in units of free electron mass) at different valleys along different directions. The GaAs X valley energy minimum is at $(0.89,0,0)(2\pi/a)$, where a is the lattice constant. Its effective mass is evaluated at this energy minimum point. All other valley minima are at their corresponding high-symmetry k points.

GaAs (100)	0.416	0.079	0.077
GaAs (111)	0.975	0.065	0.077
AlAs (100)	0.439	0.157	0.158
AlAs (111)	1.020	0.111	0.158

X valley: (100)

	Parallel: [100]	Perpendicular: [010]	Along [111]
GaAs	1.912	0.246	0.3466
AlAs	2.104	0.262	0.371

L valley: $\frac{2}{3}(111)$

	Parallel: [111]	Perpendicular: [$\bar{2}$11]	Along [100]
GaAs	1.664	0.128	0.183
AlAs	2.120	0.168	0.242

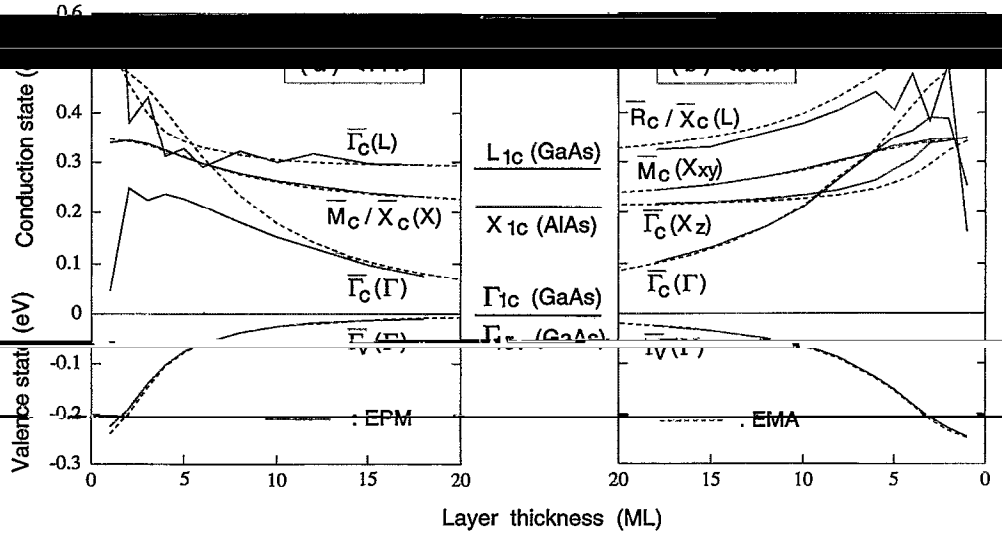

FIG. 7. Energy levels of ideal $(AlAs)_n/(GaAs)_n$ superlattices along (a) ⟨111⟩ and (b) ⟨001⟩, as a function of period n. Solid lines: pseudopotential results; dashed lines: effective-mass results. The bulk levels in the middle column are reached asymptotically as $n \to \infty$. The SL states are denoted with an over bar,

(b) SLs with laterally intermixed interfaces. Here, the

(Sec. IV B);

(c) The single δ-doping layer case. Here, a monolayer of AlAs or GaAs embedded in a perfectly ordered SL. This will establish the existence of bound states due to SL (Sec. IV C);

This case will establish the electronic structure of the

stitutional randomness, and includes the disordered SLs considered by Sasaki *et al.*,[15] and the partially ordered ones by Arent *et al.*[45] (Sec. IV E).

A. Ideal periodic AlAs/GaAs superlattices: Abrupt interfaces

pseudopotential calculated high symmetry superlattice energy levels on the period n, for (001)- and (111)-oriented SLs. The results correspond to the scalar-relativistic limit without spin-orbit interaction. Since we do not use envelope functions, the results are not limited to near zone center

agreement with previous theoretical LDA studies. We find

all period n. Both the highest valence and the lowest con-

(ii) The second conduction band at Γ, i.e., $\Gamma(L)$, is folded from the zinc-blende Γ–L_z line. For small n, this pseudodirect $\bar{\Gamma}_c(L_c)$ state mixes strongly with the direct $\bar{\Gamma}_c(\Gamma_c)$ state. The mixing, and thus the level repulsion, shows

tion of repelling states on the same or on either sublattice[52]).

(iii) For $n>6$ the X-folded, indirect $\bar{M}_c(X_z)$ conduction

middle column of Fig. 7).

The situation is very different for (001) oriented ideal

point R;

(ii) For $n<4$, the lateral $X_{x,y}$ valleys (folded to $\bar{M}$) and the X_z valley (folded to $\bar{\Gamma}$) are nearly degenerate;[54]

(iii) For $1<n\leq 8$ the pseudodirect, AlAs-like $\bar{\Gamma}_c(X_z)$ state is below the direct, GaAs-like $\bar{\Gamma}_c(\Gamma_c)$ state, thus the SL is type II;[55] for $n>8$, however, $\bar{\Gamma}_c(\Gamma_c)$ is lower, so the system is type I (experimentally, the type-II/type-I crossover is found[54] at $n \approx 11$).

compared in Fig. 7 (dashed lines) with the EPM results (solid lines). The effective masses used in the EMA are from Table I which is calculated from the EPM. At large superlattice period n, the EMA results agree very well with the EPM results. [For the (001) $\bar{R}/\bar{X}(L)$ curve, there is a small dis-

is no mixing between states from different valleys.

(iii) the potential offsets for the GaAs/AlAs interface are small (Fig. 6), thus, even for $n=1$, the k in Eqs. (12) and (13) is small, so nonparabolicity is small.

In contrast to the good agreement between EMA and EPM for the above states, the EPM $\bar{\Gamma}_c(\Gamma)$ curve for both (001) and (111) bends down at small n, while in the EMA there is a monotonic dependence. The EPM bending is due to the mixing of $\bar{\Gamma}_c(\Gamma)$ with $\bar{\Gamma}_c(X_z)$ in the (001) case and with $\bar{\Gamma}_c(L)$ in the (111) case.[52] This cannot be described by the one-band effective mass model (or even four-band $k\cdot p$

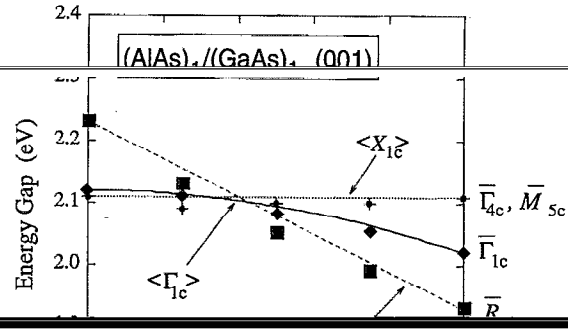

and the broken lines are linear interpolations between the respective end

given supercell. $\langle\Gamma_{1c}\rangle$, $\langle X_{1c}\rangle$, and $\langle L_{1c}\rangle$ are shown in Fig. 8 for $n=0$, 0.25, 0.50, 0.75, and for the perfect monolayer

$n\approx 0.4$, in close agreement with the LDA result[57] ($n\approx\frac{1}{3}$)

1. Intermixing in (001) superlattices

Chemical nonabruptness of interfaces in short-period superlattices has been suggested by Laks and Zunger[54] as a reason for the discrepancy between the experimental assignment of the conduction-band minimum and theoretical predictions. In particular, for the monolayer ($n=1$) superlattice

X_{xy}-derived gap at $\bar{M}$ is found.[54] We tested the idea of Laks

superlattice can be viewed as a partially ordered structure

$$(Al_{1/2+\eta/2}Ga_{1/2-\eta/2}As)_1\ (Al_{1/2-\eta/2}Ga_{1/2+\eta/2}As)_1,$$

where η is the long-range-order (LRO) parameter. $n=1$ de-

observation[54] if $n<0.4$ in the studied samples.

2. Intermixing in (111) superlattices

As the repeat period n of the ideal SL increases, chemi-

roughness in the monolayer superlattice we expand the repeat period ($X\times Y$) in the interface plane to an (8×8) unit cell. We can thus have $\eta=1-n/32$, where n is the number of Ga/Al pairs interchanged across the interface. In each set

the band gaps can shift considerably. We have considered the $(AlAs)_6/(GaAs)_6$ (111) SL, because of a controversy about the nature of the band gap between theory[52,60]

theory predicts a direct band gap if the interfaces

next interface. As a result, there is in principle no periodicity

however, we assume a repeat period of 4 ML along [001], resulting in a 512 atom supercell. Hence, within the supercell there are four distinct Al-rich and four distinct Ga-rich layers with compositions $0.5+\eta/2$ and $0.5-\eta/2$, respectively.

The energy eigenvalues of the large supercell are analyzed in terms of their "parent" zinc-blende states from

expanded in terms of a usually small number of zinc-blende wave functions. We use the expansion coefficients of the latter expansion as weights in evaluating spectral averages of zinc-blende-like eigenvalues.[59] For example, $\langle\Gamma_{1c}\rangle$ denotes the expectation value of the zinc-blende Γ_{1c} energy level in a

SL, we have used a planar (4×4) unit cell to simulate chemical intermixing within ± 1 ML across the interfaces, resulting in a 384 atom 3D unit cell. The superlattice is thus converted

AlAs layers, and two alloy layers. We chose the composition of the alloy layers to be 50%, corresponding to maximum

the pseudodirect $\bar{\Gamma}_{6c}(L_{6c})$ and indirect gaps $\bar{M}_{6c}(X_{6c})$

however, does not change upon intermixing, remaining $\bar{\Gamma}_{6c}(\Gamma_{6c})$ although the pseudodirect transition $\Gamma_{6c}(L_{6c})$ is now only 20 meV (down from 50 meV) away.

TABLE II. Band gaps (in eV) of the $(AlAs)_6/(GaAs)_6$ (111) superlattice with ideal and chemically intermixed interfaces. The zinc-blende (ZB) parent states are found by projecting the SL wave functions on ZB states.

Gap (ZB origin)	Ideal SL	Intermixed
$\bar{\Gamma}_{6c}(\Gamma_{6c})$	1.81	1.89
$\bar{\Gamma}_{6c}(L_{6c})$	1.86	1.91
$\bar{M}_{6c}(X_{6c})$	1.92	1.95
$\bar{M}_{6c}(L_{6c})$	2.02	2.04

Experimentally, the absorption edge was determined to be at 1.90 eV,[61] close to our calculated band gap of the intermixed SL. The observed PL emission peak at 1.80 eV, however, cannot be explained by chemical intermixing: Table II shows that intermixing leads to a blue shift while experimentally the PL is red shifted. A possible explanation for a large red shift of the PL emission is offered in Sec. IV E, where it is

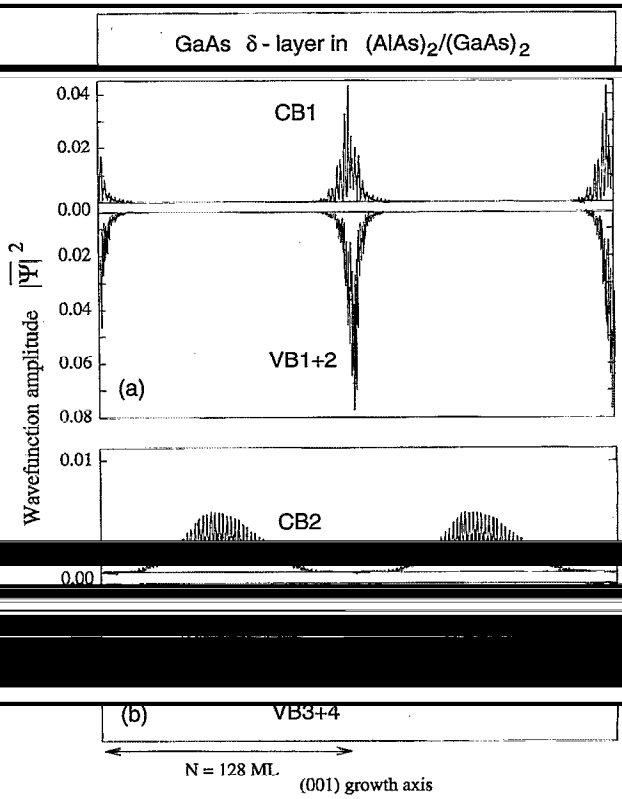

FIG. 9. Pseudopotential calculated planar average of the wave functions

C. A single δ layer inside an ordered superlattice

We next model the case of a single layer of A or G inserted in an ordered A_2/G_2 SL. It is well known[62] that, while in 3D an impurity potential has to exceed a certain

bound state. To understand the possibility of impuritylike localization, consider, for example, a G_3 δ layer embedded in the otherwise perfect o-SL $\cdots A_2G_2A_2G_2A_2G_2\cdots$, thus converting it into $\cdots A_2G_2A_2G_3A_2G_2\cdots$, denoted as $A_2/G_2{:}G_3$. If the G_3 δ layer is attractive to electrons (holes) it will bind a state below the CBM (above the VBM) of the o-SL.[63] We find that a $(GaAs)_3$ δ layer in the $(AlAs)_2/(GaAs)_2$ o-SL indeed binds an electron and a (double degenerate) hole [Fig. 9(a)], while an $(AlAs)_3$ layer binds an electron but does not bind a hole (Fig. 10). Figure 11 shows as dashed lines the dispersion of the bound states of a single δ layer in A_2/G_2,

of the $n=2$ ordered SL along the symmetry lines $\bar{\Sigma}$ and $\bar{\Delta}$, i.e., from $\bar{\Gamma}$ to $\bar{M}=1/\sqrt{2}(1,1)$ and from $\bar{\Gamma}$ to $\bar{X}=1/\sqrt{2}(1,0)$, respectively. The thin horizontal lines denote the band edges

therefore correspond to a "bound state." For the δ layer, we

while those of $A_2/G_2{:}A_3$ are $\Delta\varepsilon_e=33$ and 5 meV, respectively. The hole binding energy of $A_2/G_2{:}G_3$ is $\Delta\varepsilon_h=37$

$(GaAs)_2/(AlAs)_2$ are extended states, as illustrated in Fig. 9(b) for the next higher (lower) state following the bound electron (hole) in $A_2/G_2{:}G_3$.

The wave-function localization perpendicular to the

lowing length scales (in ML units). The effective localization length for wave function ψ_E at energy E is defined as[64]

$$L_{\text{eff}}(E)=\frac{1}{d}\left[\int dz\left(\int dx\,dy|\psi_E(\mathbf{r})|^2\right)^2\right]^{-1}, \tag{16}$$

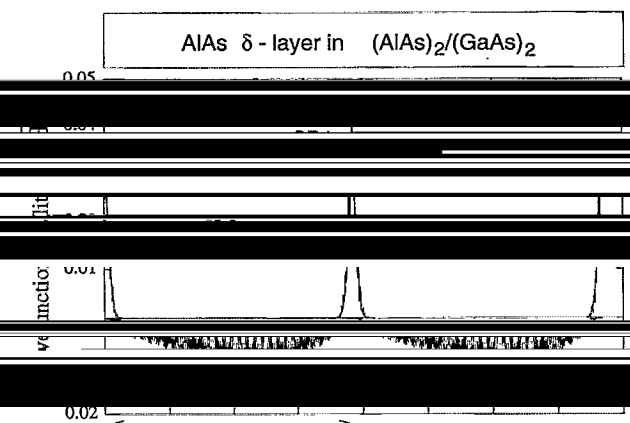

FIG. 10. Like Fig. 9, but for an $(AlAs)_3$ δ layer. In this case, there is no

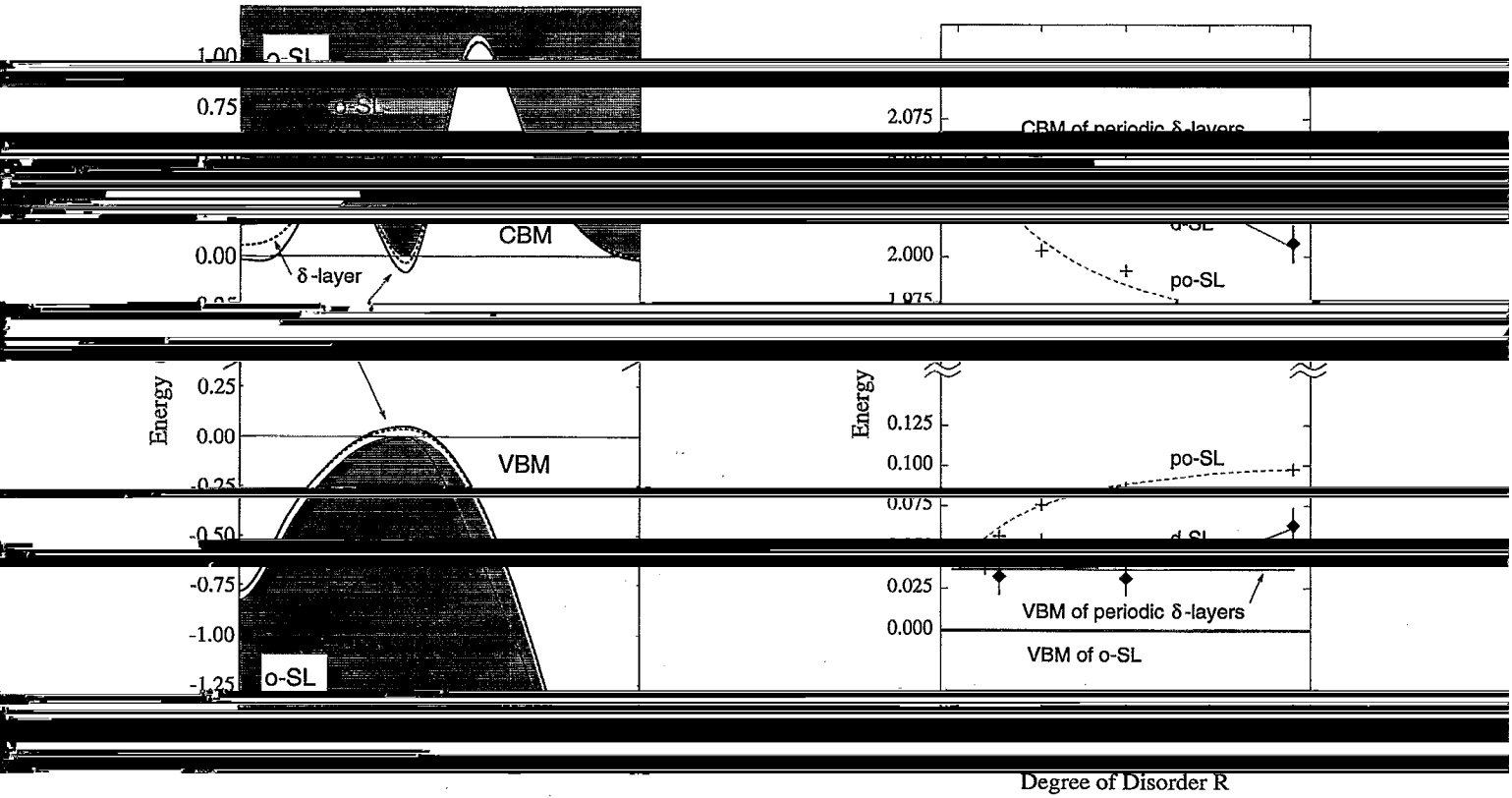

supercell size is $N=128$.

function of R [Eq. (3)]. Lines are guides to the eye. The thick horizontal lines denote the unperturbed band edges of the parent o-SL. The vertical bars on the d-SL data points denote the range of binding energies obtained from ~10 different realizations of a d-SL with length $N=128$.

and measures the region along z where ψ_E is "sizeable." In Eq. (16) the planar average of $|\psi_E|^2$ is taken before integrating along z, d is the monolayer thickness, and the wave function is assumed to be normalized in the volume of the

similar to those obtained in the fully disordered SL, suggesting that the same mechanism of localization could be at work

has $L_{\text{eff}}=1$. The asymptotic decay length γ^{-1} far away from the localization region is given by $\langle|\overline{\psi_E(z)}|\rangle \propto e^{-\gamma z}$, where

D. An ordered array of δ layers inside an ordered superlattice

TABLE III. Effective localization length L_{eff} [Eq. (16)] and exponential decay length γ^{-1} for the δ-layer systems depicted in Figs. 9 and 10, and the disordered and partially ordered SLs depicted in Figs. 15 and 16, respectively. Reported are the values for the states at the conduction-band minimum (CBM) and at the valence-band maximum (VBM) in ML units.

as the thin solid line in Fig. 12. We see that even for an array of closely spaced δ layers ($R\to 1$) the binding energy does not increase, indicating negligible interaction between the neighboring, coherently arranged bound states. In fact, at

those of a disordered system. Consequently, short supercells

TABLE IV. Overview of different disordered systems [superlattices (SL) and multiple quantum wells (MQW)] in the parameter space of R [Eq. (3)] and $\Delta n/n$.

	Small mean density	Large mean density
Small fluctuation ($\Delta n \ll n$)	nearly "ideal" SL/MQW impuritylike localized states	strongly disordered MQW effective-mass-like bound states
Large fluctuation $n<10$	Strong perturbation of band edges	d-SL, po-SL

with $N \approx 10$–20, as have been used before to describe disordered SLs,[39] are unable to simulate the behavior of truly

E. A disordered array of δ layers

Next, we introduce disorder in the SL by arranging the δ

that very large supercells are required, if one wishes to accurately describe the layer–layer correlation function of a disordered system. We have used total lengths N of up to 1000 ML for EPM, and up to 2000 ML for EMA calculations, in order to verify the convergence of the results ob-

est needs to be evaluated; in some cases (see below) we have used ~10 realizations of a d-SL of given total length N and disorder parameter R, and have found that the EPM-

lengths) have very small fluctuations. Therefore, we have often used a single realization of a d-SL to calculate band-edge energies and wave functions. For the EMA-calculated density of states, on the other hand, we have performed con-

In the following, we discuss separately two regimes of

thickness fluctuations Δn are of the same order as the unperturbed thickness, i.e., $\Delta n \approx n$. This case includes the d-SLs of Sasaki *et al.*[45] and the po-SLs of Arent *et al.*[46] Second, we treat the case where the thickness fluctuations are relatively small perturbations of the ideal SL, i.e., $\Delta n \ll n$. An overview of the different regimes considered is given in Table IV.

1. Disordered SLs with $\Delta n \approx n$: EMA density of states

To calculate the spectral properties of a d-SL over a large energy range, we use the effective-mass model described in Sec. III B. The advantage of the EMA method is that we can easily calculate a large number of eigenstates (not only near-gap states). This permits obtaining a good

properties. We have thus modeled a 2000 ML Sasaki-type

edges. We calculated heavy-hole states for the hole and X

13. Each state is represented by a single horizontal line. The vertical position of the line indicate its energy and horizontal

line is $2L_{\text{eff}}$ using the one-dimensional version of Eq. (16). Figure 13 shows that all states are localized, as expected

There is no transition from localized states to delocalized states. Around the band edge, the localization of the states is

gives the distribution of the d-SL states, in both energy and

One way to display the information in Fig. 13 more quantitatively is to calculate the density of states (DOS) and localization length L_{eff} as functions of energy E. We have calculated 100 d-SL systems (each with 2000 ML as in Fig.

one-dimensional DOS. If the lateral dimensions were considered, the shapes of the DOS would change.) For electron states, we calculated both the X valley states and Γ valley

only makes sense for low-energy regions where two separate valleys are well defined. For high-energy regions, the states from X and Γ valleys may not be distinguishable, and thus

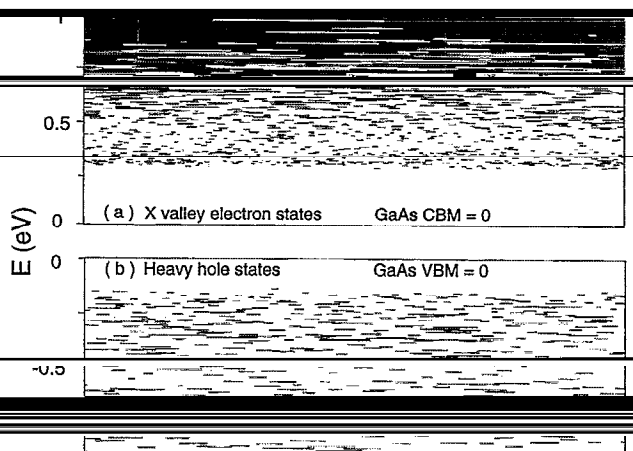

FIG. 13. Effective-mass calculated localized states of a 2000 ML d-SL.

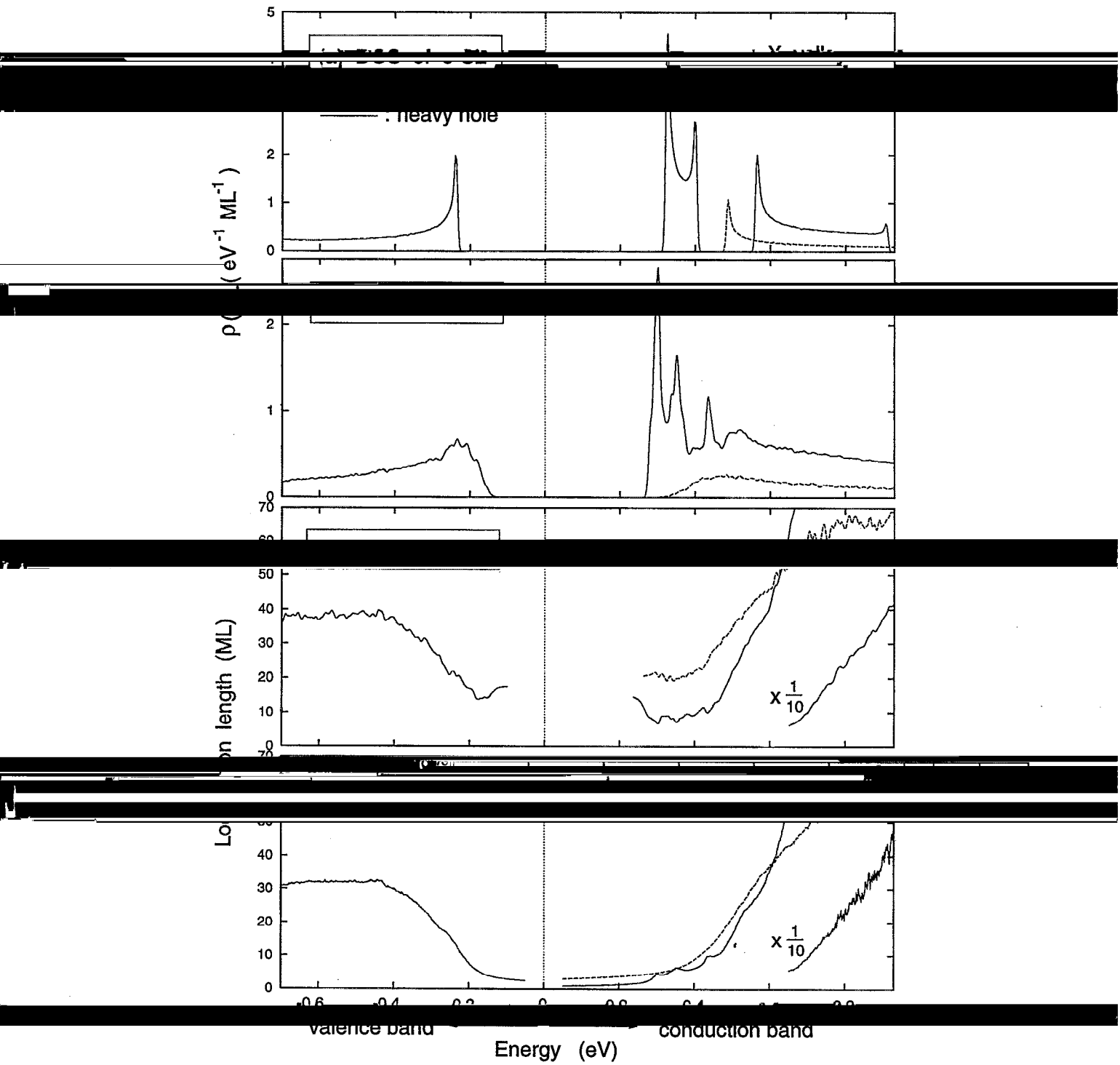

FIG. 14. Effective-mass calculated density of states of (a) the (001)-ordered $(GaAs)_2/(AlAs)_2$ and (b) Sasaki-type disordered superlattices, and the localization lengths (c) L_{eff}, (d) γ^{-1} of the disordered superlattice. The conduction-band energy is measured from the bulk GaAs CBM and the valence-band energy is measured from the bulk GaAs VBM.

a multiband calculation. A very interesting fact is the peaks in the DOS of X valley electronic states. To understand these peaks, we have calculated the DOS for the $(GaAs)_2/(AlAs)_2$ ordered superlattice. The results are shown in Fig. 14(a). It is evident that the peaks of X valley states of the d-SL in Fig. 14(b) are the remnants of the peaks seen in Fig. 14(a) for the o-SL with some shifts. On the other hand, for Γ valley states and heavy-hole states, there is only one peak in the ordered superlattice, thus their DOS of d-SL have simple structures.

The effective localization length L_{eff} [Eq. (16)] is shown in Fig. 14(c). Notice that L_{eff} increases a bit near the band edge. As described by the Lifshits theory, this phenomenon is due to consecutive wide potential wells. At energy far away from the band edge, L_{eff} of the X valley electron states and

heavy-hole states bend down. Part of the reason is that we used the boundary condition of Eq. (9). As a result, for very large E, when the effect of the potential is no longer important, the mass confinement still plays an important role. This

length γ^{-1} as described in Sec. IV C. It turns out that this γ is just the exponential growth rate of $A_{N+1}(E)$ [defined in Eq. (14), which does not equal A_1 for arbitrary E] as a function of N. If E is an exact eigenvalue ϵ_i of an localized state, then $A_{N+1}=A_1$, thus, the magnitude of A_{N+1} is O(1). However, the measure of these $E\in\{\epsilon_i\}$ is zero, so in most cases $A_{N+1}\propto e^{\gamma N}$. Using this fact, we can calculate $\gamma(E)$ from $A_{N+1}(E)$ directly and the result is accurate and reliable. The $\gamma^{-1}(E)$ are shown in Fig. 14(d). Note that, in the DOS tail region, $L_{\rm eff}$ is larger than $2\gamma^{-1}$, indicating Lifshits localiza-

This can be understood by the fact that $L_{\rm eff}\sim 3\gamma^{-1}$ for a localized wave function $\cos(kz)e^{-\gamma|z|}$ with k much larger than γ. In Figs. 14(a) and 14(d), corresponding to the peaks of DOS for X valley states, its $L_{\rm eff}(E)$ and $\gamma^{-1}(E)$ show dips

the dips of $L_{\rm eff}(E)$ and peaks of $\gamma^{-1}(E)$ can be understood as follows. The existence of the eigenstates around a given energy E will slow down the exponential growth of

O(1)], thus $\gamma^{-1}(E)$ increases. So a peak in the DOS will induce a peak in $\gamma^{-1}(E)$. On the other hand, because of

2. Disordered SLs with $\Delta n\approx n$: Band-edge states and oscillator strength

We now focus on the band edges near the band-gap region. The

and emission in the visible-light and near-infrared regions, and thus determine the optoelectronic properties of the d-SLs. First, we discuss the results of our pseudopotential calculations. In Fig. 11 we show the EPM-calculated dispersion of the band-edge states of the d-SL (solid lines) with $p(1)=p(2)=p(3)=\frac{1}{3}$ along the symmetry lines $\bar{\Sigma}$ and $\bar{\Delta}$. The thin horizontal lines denote the band edges of the under-

("binding energy") increases in the order $\bar{M}\to\bar{\Gamma}\to\bar{X}$. The large binding energy at $\bar{\Gamma}$ is a consequence of the level repulsion of the folded L_{1c} states, which is much stronger for odd values of the repeat period n than for even n [see Fig. 7(b)]. In the d-SL the odd–even selection rule is broken, leading to a stronger level repulsion in the d-SL than in the

the conduction-band edge below the ones at $\bar{X}$ and $\bar{M}$ by 60 meV, making the d-SL a direct-gap material, even though the o-SL is indirect (with CBM at $\bar{M}$).

In order to establish whether the direct transition does indeed lead to efficient recombination, we have to consider

show a few band-edge wave functions of an $N=1000$ ML d-SL, which are plotted using the planar average introduced in Fig. 9. For example, the states labeled CB3 and VB1 are localized at the same positions along the chain, and consequently their dipole matrix element can be large, whereas

tor strength f of an optical transition, which is defined as

$$f=\frac{1}{\hbar\omega}\frac{2|\langle c|\mathbf{p}|v\rangle|^2}{3m}. \tag{17}$$

Here $\hbar\omega$ is the transition energy, $\langle c|\mathbf{p}|v\rangle$ the dipole matrix element between states $|c\rangle$ and $|v\rangle$, and m the free electron mass. The factor of 3 in the denominator is introduced to average over the three polarizations x,y,z. In Table V we report calculated values of f for direct transitions in various

(i) dered SLs are 1–2 orders of magnitude smaller than those of the (higher energy) direct transitions.

(ii) The transition between an extended state and a localized

is of the similar strength as a pseudodirect transition,

(iii) Transitions between two states that are localized in the same region along z are of comparable strength

Thus, the transition between the two localized states VB1 and CB3 in Figs. 15(c) and 15(d) is truly direct, rather than pseudodirect. The latter result explains the experimentally

late $\tau=1$ ns for the VB1→CB3 transition at energy 1.96 eV. These radiative lifetimes are 1000× faster compared to those measured in indirect-gap o-SLs ($\tau\approx 5.5$ μs at $T=2$ K).[54] Furthermore, the calculated transition energy agrees very well with measured PL emission lines in d-SLs, which were found at ~1.96 eV.[65]

We have seen that in ordered SLs the distinction between direct and pseudodirect transitions can be made by mapping SL states on "parent" states in the zinc-blende structure: Pseudodirect transitions at a SL wave vector $\bar{\mathbf{K}}$ involve one folded state and one state genuine to $\bar{\mathbf{K}}$. An example is the

(the height of the d-SL Brillouin zone is equal to $2\pi/Nd$), the parentage of a d-SL state can still be defined in terms of its projection on zinc-blende states. We have performed such an analysis for a few conduction-band-edge states in (001) d-SLs. We found two types of states:

(i) localized states whose projection on zincblende (ZB) states is peaked at the Γ point, and

(ii) localized states whose projection is peaked at the X_z point of the ZB Brillouin zone.

In real space, the Γ like states are localized in GaAs-rich regions [e.g., where a few $(GaAs)_n$ layers are separated by

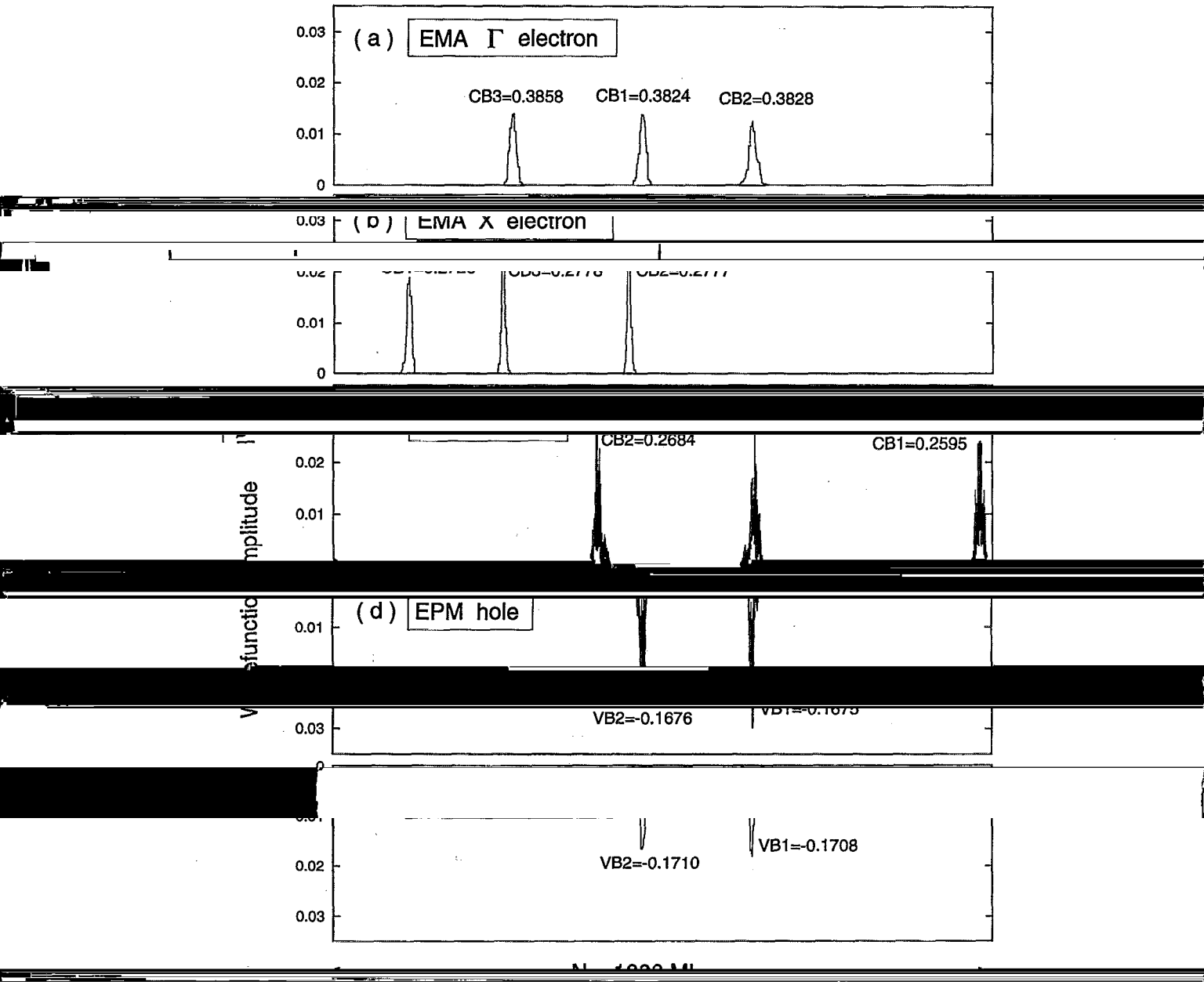

FIG. 15. The valence-band maximum states and conduction-band minimum states of a 1000-ML disordered superlattice, obtained by empirical pseudopotential model (EPM) and effective-mass approximation (EMA). The numbers are the eigenenergies of the states in eV. For the conduction-band states and valence-band states, they are measured from bulk GaAs CBM and VBM, respectively.

type-II band alignment of the ordered (001) SLs. Unlike in

are Γ-like]. Note that the 1×1 *o*-SL also has the $\Gamma(\Gamma_{1c})$ state below the $\bar{\Gamma}(X_z)$ state [Fig. 7(b)]. This band order is not reproduced by the EMA, and we see below that also for the

mechanism of localization in both cases is essentially the

concentration of δ layers, an increasing number of bound states is introduced, which are degenerate at small concentration R. Unlike in the case of the periodic array of δ layers,

TABLE V. Oscillator strengths of direct optical transitions in bulk materials

valence-band maximum (in case of a degenerate VBM the squared dipole matrix elements are averaged over the degenerate manifold). For the disordered systems, the final states are identified in Figs. 9, 10, 15, and 16, respectively.

System	Final state	Energy (eV)	f
Bulk GaAs	Γ_{1c}	1.52	4.03
[illegible]	[illegible]	[illegible]	[illegible]
[illegible]	[illegible]	[illegible]	[illegible]
$(AlAs)_2/(GaAs)_2$	$\Gamma(X_z)$	2.09	0.08
[illegible]	[illegible]	[illegible]	[illegible]
GaAs δ layer	CB1	2.04	1.67
[illegible]	[illegible]	[illegible]	[illegible]
d-SL	CB3	1.96	1.68
po-SL	CB1	1.87	2.76

[illegible] labels are localized at the same positions along z, i.e.,

16];

(ii) the band-gap reduction is slightly larger for the po-SL than for the d-SL at equal R (see Fig. 12).

Indeed, PL emission lines have been measured at energies as low as 1.87 eV,[66] in agreement with our calculated band gap of 1.87 eV. The CB1 and VB1+2 states are localized in a region where five $(GaAs)_3$ wells are separated by four

[illegible] localized in region with four 3 ML AlAs/GaAs wells separated by

[illegible] density of such a one-dimensional clustering is larger than in the d-SL. For example, the probability to find the next

distribution function of the po-SL leads to LRO (see Fig. 4), which causes an enhancement of the structure factor $|S(k_m)|^2$ at certain wave vectors (Fig. 5). The structure factor enters

rational averages give the size of the fluctuations of the [illegible]. It is interesting to note that the band tail in

theory, which could also explain why LRO present in the [illegible] spect to the d-SL.

trons. This asymmetry is contrary to expectations based on 1D one-band models, and reflects the strong band coupling and 3D character retained in our calculation. In a one-band

Next, we calculate the Sasaki-type d-SL using the effective-mass model. The EMA results are also shown in

because the kinetic energy becomes increasingly dominant

band-edge states for the holes: The highest hole states are

Also shown in Fig. 12 are the band-edge energies of the partially ordered SL (po-SL), which was studied experimentally by Arent *et al.*[45] The corresponding wave functions are depicted in Fig. 16. While the trends are similar to those observed in the d-SLs two distinct features are noteworthy:

(i) Occupied and unoccupied levels with corresponding

wave-function shape; the eigenenergies differ by only 3 meV. The wave functions are localized at positions where consecutive wide GaAs wells are separated by thin AlAs barriers.

For electron states, the situation is more complicated. For EMA states, again, the location of the localized states is simply determined by the geometry of the potential. For example, the EMA Γ valley states in Fig. 15(a) are localized where a few consecutive wide ($n=3$) GaAs wells are separated by thin ($n=1$) AlAs barriers. Thus, these EMA Γ valley states have the same locations as the EMA hole states, as

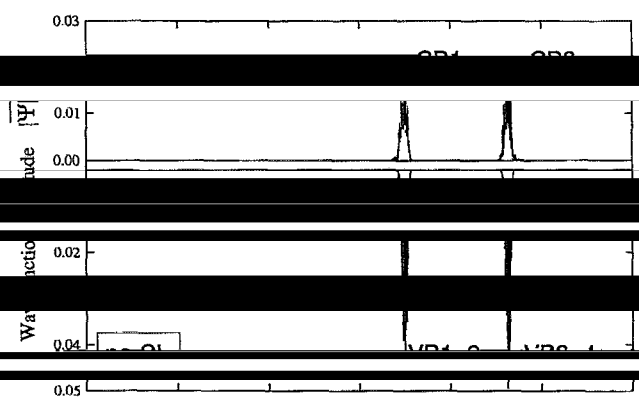

FIG. 16. Pseudopotential calculated planar average of the wave functions squared in a 1000 ML partially ordered SL (po-SL). Unoccupied states are labeled CB1, CB2,...; occupied states are labeled VB1, VB2,..., and are [illegible]

states [Fig. 15(b)], on the other hand, are localized where a few consecutive wide ($n=3$) AlAs wells are separated by thin ($n=1$) GaAs barriers. From the EMA calculations one

the Γ valley derived states. The projection analysis described above showed that the EPM conduction band edge states are more Γ like than X like states. This is at variance with the EMA results: The d-SL has a pseudodirect band gap in the

description.[67] However, for the wave functions we do get an

derived CB2 state in Fig. 15(a). Thus, the EMA can still be useful to describe some properties of the electron state in the d-SL. The fact that we do not get agreement for all other CBM states indicates that the EPM results are complicated by possible Γ–X coupling.

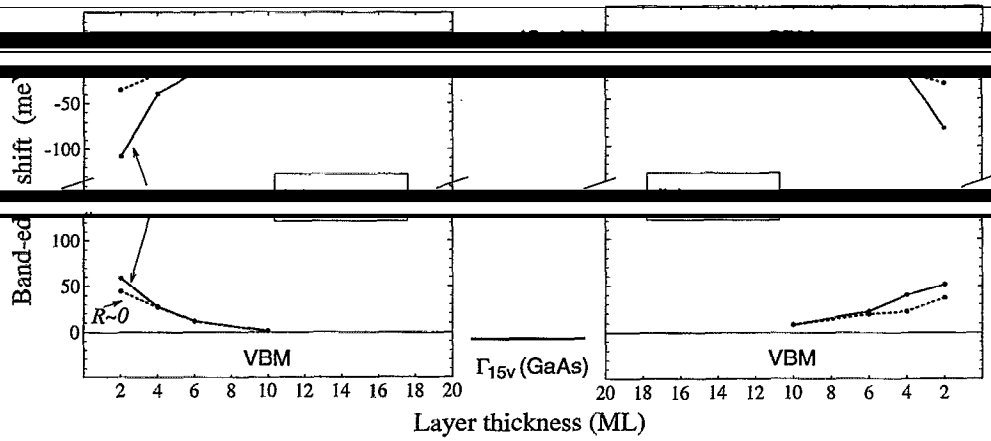

FIG. 17. Pseudopotential calculated gap levels in the presence of 1 ML thickness fluctuations in $(AlAs)_n/(GaAs)_n$ superlattices along (a) ⟨111⟩ and (b) ⟨001⟩, as a function of period n. Energies are measured with respect to the band extrema of the ideal $n\times n$ SL (see Fig. 7). $R=1$ and $R\to 0$ denote, respectively, the concentrated and dilute limit of chain mutations [Eq. (3)].

2. Disordered SLs with $\Delta n \leq n$

Fig. 17 relative to the band edges of the ideal SLs (the energy zero, see Fig. 7). We see that:

(i) The band-gap reductions $\Delta E_g = \Delta\varepsilon_e + \Delta\varepsilon_h$ decay

direction; they are 166, 67, 29, and 14 meV for $n=2$, 4, 6, and 10 in the ⟨111⟩ direction, and 133, 64, 36, and 27 meV in the ⟨001⟩ direction, respectively.

("band-gap pinning") of the number of chain mutations.

In order to explain these findings, we discuss the intermediate case of the $n=6$ ⟨111⟩ SL, where the VBM is already pinned (independent of R), but where the CBM still shows dispersion with R (see Fig. 17). Figure 18(a) shows the CBM and VBM wave functions for the $R=1$ SL. The

minimal amplitude in the AlAs barriers and maximal amplitude on the two neighboring mutated (7 ML) GaAs wells ("twin" fluctuation denoted by bold arrows). The CBM also resembles a bound state in a coupled double quantum well. The hole wave function at the VBM is likewise localized on a number of mutated 7 ML GaAs wells [Fig. 18(a)]; in contrast to the CBM, however, the VBM wave function is localized on

tern of the VBM wave function is that these states are in fact decoupled, quantum-well confined states, which are degenerate in energy within the accuracy of our calculation (≲0.1 meV). A typical hole and electron wave function localized on an isolated $(GaAs)_7$ mutation in an otherwise ideal 6×6 ⟨111⟩ SL are shown in Fig. 18(b). We see that the hole wave

concentrated ($R=1$) mutations [Fig. 18(a)], and its binding energy $\Delta\varepsilon_h(R\to 0)=11$ meV equals the value at $R=1$. At the CBM, the larger penetration of the wave function into

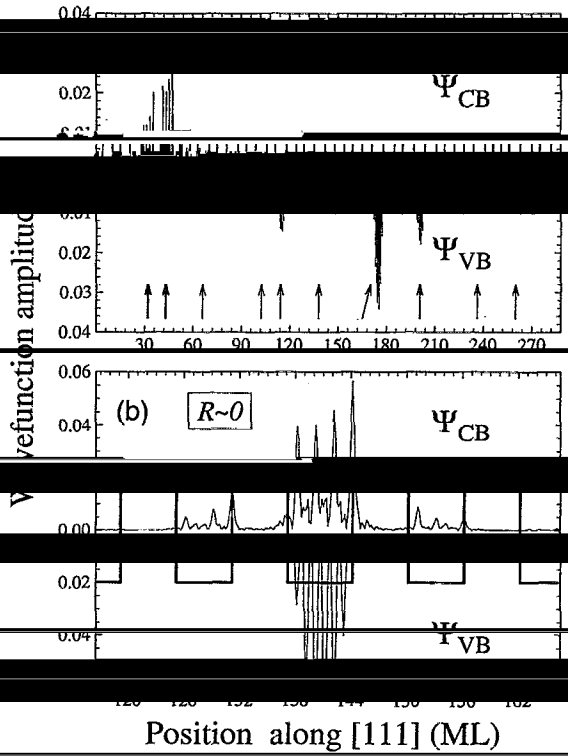

FIG. 18. Pseudopotential calculated planar averages of wave functions squared of the CBM and VBM in the $(AlAs)_6/(GaAs)_6$ SL along ⟨111⟩ with ±1 layer-thickness fluctuations. Hole wave functions are plotted in the

a 6×6 SL host. The rectangular lines show the growth sequence of the SL, with GaAs layers represented by wells, and AlAs layers represented by barriers, respectively. The vertical arrows in (a) indicate the 7-ML-thick, "mutated" wells.

states should be observable as photoluminescence centers whose energy is below the absorption edge of the underlying "ideal" SL structure. This photoluminescence will lack phonon lines because the optical transitions are direct in the good quantum number), and because the k_z selection rule is relaxed by vertical disorder. Indeed, while we have shown in Sec. IV A that ideal ⟨111⟩ $(AlAs)_n/(GaAs)_n$ SLs have a direct band gap with a type-I band arrangement, Cingolani and co-workers[61] noted a ~100 meV red shift of the photoluminescence at 1.80 eV relative to the absorption in $(AlAs)_6/(GaAs)_6$ (111) SLs, interpreting this as reflecting a type-II band arrangement. However, we have noted that the red-shifted photoluminescence originates from thickness-fluctuation bound states. Our calculated band gap of the $n=6$ superlattice with ± 1 ML thickness fluctuations is 1.78 eV for $R=1$, and 1.80 eV for $R\to 0$, close to their observed photoluminescence peak position (1.80 eV).[61] Recall that chemical intermixing leads to a blue shift of the band gap (see Table II), whereas larger thickness fluctuation is needed to explain the observed 100 meV red shift.

Figure 17 shows that the bound states of isolated mutations ($R\to 0$) merge with those of concentrated layer-thickness fluctuations ($R\to 1$) at some pinning period n_p. At this point the band-gap reduction is pinned at the value

$$\Delta E_g(R)=\lim \Delta E_g(R)=\Delta\varepsilon_e+\Delta\varepsilon_h, \tag{18}$$

where $\Delta\varepsilon_e$ ($\Delta\varepsilon_h$) is the electron (hole) binding energy of an isolated ($R\to 0$) layer mutation. Qualitatively, Eq. (18) can be understood in terms of the 1D effective-mass picture (Sec. III B). Each of the $(n+1)$ ML mutations gives rise to a bound state below the band edge of the $n\times n$ SL.[20,14] For very large n, when the quantum wells are completely decoupled (the tunneling probability and, hence miniband width, decrease exponentially with n), the SL energy spectrum is simply that of degenerate single quantum wells of thicknesses n' with eigenenergies $\varepsilon_\nu(n')$. Hence, the extra binding energy of an $(n+\Delta n)$ ML mutation approaches asymptotically

where $\varepsilon_0(n)$ is the ground-state energy of a carrier with mass m^* in an n-ML-wide quantum well, which scales like $1/m^*n^2$ for [illegible]. Rather than a fixed Δn, we obtain from the first equality of Eq. (19) $\Delta\varepsilon_e=10.0$, 2.4, and 0.7 meV for $n=20$, 50, and 100 in the (111) SL [the last equality of Eq. (19) gives 14.3, 3.0, and 0.8 meV, respectively]. The band-gap reduction for a [illegible]

V. CONCLUSIONS

Our main conclusions can be summarized as follows.

(a) (001)-ordered superlattices:

(i) The $n=1$ SL has an indirect band gap at $\bar{R}$; Insufficient interfacial abruptness in the experimentally studied samples[54] leads instead to an X-derived CBM.

(ii) For $n\le 4$, the $\bar{M}(X_z$-folded) states and the $\bar{\Gamma}(X_z$-folded) states are nearly degenerate;

(iii) The crossover from AlAs-like $\bar{\Gamma}_{1c}(X_z)$ (type II) to GaAs-like $\bar{\Gamma}_{1c}(\Gamma_{1c})$ (type I) happens around $n=8$.

(b) (111)=ordered superlattices:

(i) $\bar{\Gamma}_{1c}(\Gamma_{1c})$ is the CBM (type I) for all n;

(ii) There is a strong even–odd oscillation of the CBM energy due to mixing.

ordered SLs, Cingolani and co-workers[61] found for $n=6$ a type-II SL with a ~100 meV red shift between absorption and PL; we find that lateral interfacial intermixing can not explain this discrepancy, but monolayer thickness fluctuations in the measured sample do resolve the disagreement.

(c) Single δ layer doping in o-SL:

(i) A $(GaAs)_3$ δ layer in $(GaAs)_2/(AlAs)_2$ (001) SL produces an electron and a hole bound state with binding energies $\Delta\epsilon_e=18$ meV and $\Delta\epsilon_h=37$ meV, respectively;

(ii) An $(AlAs)_3$ δ layer in $(GaAs)_2/(AlAs)_2$ (001) SL pro-

(d) An ordered array of δ layers:

The bound states in neighboring δ layers start to have large interaction when their distance is less than 20 ML.

(e) A disordered SL with $\Delta n\approx n$ (i.e., $n=1,2,3$):

(i) There is a 130 meV red shift in the band gap compared with the o-SL;

(ii) The conduction-band minimum is at $\bar{\Gamma}$, not at $\bar{X}$, as for the $n=2$ o-SL

(iii) The conduction-band-edge states are more Γ-like than X-like, thus the oscillator strength is as large as the pair;

(iv) The band-edge state localization length of the d-SL is about the same (20 ML) as the δ layer bound state;

(v) The localization lengths increase as the energy moves [illegible] there is no mobility edge;

(vi) The DOS of the d-SL has a peak near the edge of o-SL DOS and has a tail into the band-gap region; if

(f) A disordered SL with $\Delta n\ll n$:

For $\Delta n=1$ and $n>6$, the band-edge energies are nearly pinned at their δ doping level, independent of the magnitude of the disorder.

ACKNOWLEDGMENTS

The authors thank Dr. S. H. Wei for many helpful discussions and advice. This work was supported by the office of Energy Research, Materials Science Division, U.S. Department of Energy, under Grant No. DE-AC02-83CH10093.

[1] A. Ourmazd, D. W. Taylor, J. Cunningham, and C. W. Tu, Phys. Rev. Lett. **62**, 933 (1989).

[3] B. Jusserand, F. Mollot, R. Planel, E. Molinari, and S. Baroni, Surf. Sci. **267**, 171 (1992).

[4] R. M. Feenstra, D. A. Collins, D. Z.-Y. Ting, M. W. Wang, and T. C. N. Miller, J. Vac. Sci. Technol. B **5**, 1191 (1987).

[7] R. F. Kopf, E. F. Schubert, T. D. Harris, and R. S. Becker, Appl. Phys. Phys. Lett. **58**, 2755 (1991).

[9] C. Parks, A. K. Ramdas, M. R. Melloch, and L. R. Ram-Mohan, Phys. Rev. B **48**, 5413 (1993).

[10] J. R. Meyer, A. R. Reisinger, K. A. Harris, R. W. Yanka, and L. M. Mohnkern, Appl. Phys. Lett. **64**, 545 (1994).

[11] J. D. Dow, S. Y. Ren, and K. Hess, Phys. Rev. B **25**, 6218 (1982).

[12] S. Das Sarma, A. Kobayashi, and R. E. Prange, Phys. Rev. Lett. **56**, 1280 (1986).

[13] R. Merlin, K. Bajema, R. Clarke, F.-Y. Juang, and P. K. Bhattacharya, Phys. Rev. Lett. **55**, 1768 (1985).

[14] A. Chomette, B. Deveaud, A. Regreny, and G. Bastard, Phys. Rev. Lett. **57**, 1464 (1986).

[15] A. Sasaki, M. Kasu, T. Yamamoto, and S. Noda, Jpn. J. Appl. Phys. **28**,

[16] C. A. Warwick and R. F. Kopf, Appl. Phys. Lett. **60**, 386 (1992).

[17] V. I. Belitsky, T. Ruf, J. Spitzer, and M. Cardona, Phys. Rev. B **49**, 8263 (1994).

[18] Q. A. Wang, W. W. Lee, A. Ourmazd, and T. D. Harris, Appl. Phys. Lett.

M. J. S. P. Brasil, A. A. Bernussi, M. A. Cotta, M. V. Marquezini, J. A.

[20] R. K. Littleton and R. E. Camley, J. Appl. Phys. **59**, 2817 (1986).

[21] H. X. Jiang and J. Y. Lin, Superlattices and Microstructures **3**, 689 (1987).

[22] R. A. Davies, M. J. Kelly, and T. M. Kerr, Appl. Phys. Lett. **53**, 2641 (1988).

[23] H. D. Rees, Appl. Phys. Lett. **55**, 1114 (1989).

(1992).

Sci. Technol. A **11**, 923 (1993).

[28] M. Proctor, G. Oelgart, H. Rhan, and F.-K. Reinhart, Appl. Phys. Lett. **64**, 3154 (1994).

[29] P. W. Anderson, Phys. Rev. **109**, 1492 (1958).

[30] I. M. Lifshits, Sov. Phys. JETP **17**, 1159 (1963).

[31] P. A. Lee and T. V. Ramakrishnan, Rev. Mod. Phys. **57**, 287 (1985).

[32] P. Phillips, Ann. Rev. Phys. Chem. **44**, 115 (1993).

[33] I. M. Lifshits, S. A. Gredeskul, and L. A. Pastur, *Introduction to the Theory of Disordered Systems* (Wiley, New York, 1987).

[34] R. E. Borland, Proc. R. Soc. London Ser. A **274**, 529 (1963).

[35] F. Laruelle and B. Etienne, Phys. Rev. B **37**, 4816 (1988).

[36] K. Hirose, D. Y. K. Ko, and H. Kamimura, J. Phys. Condens. Matter **4**,

[37] D. B. Laks, S.-H. Wei, and A. Zunger, Phys. Rev. Lett. **69**, 3766 (1992).

[38] E. G. Wang, J. H. Xu, W. P. Su, and C. S. Ting, Appl. Phys. Lett. **63**, 1411 (1993).

[39] E. G. Wang, J. H. Xu, W. P. Su, and C. S. Ting, Appl. Phys. Lett. **64**, 443

E. G. Wang, W. P. Su, and C. S. Ting, J. Appl. Phys. **76**, 3064 (1994).

[41] V. Kumar and G. Ananthakrishna, Phys. Rev. Lett. **59**, 1476 (1987).

[42] X. Chen and S. Xiong, Phys. Rev. B **48**, 5273 (1993).

[43] M. Kasu, T. Yamamoto, S. Noda, and A. Sasaki, Appl. Phys. Lett. **59**, 800

[45] D. J. Arent, R. G. Alonso, G. S. Horner, D. Levi, M. Bode, A. Mascaren-

[46] T. Yamamoto, M. Kasu, S. Noda, and A. Sasaki, J. Appl. Phys. **68**, 5318

R. A. Mäder, L.-W. Wang, and A. Zunger, Phys. Rev. Lett. **74**, 2555 (1995).

[48] K. A. Mäder and A. Zunger, Phys. Rev. B **50**, 17 393 (1994).

[49] L.-W. Wang and A. Zunger, J. Chem. Phys. **100**, 2394 (1994).

[50] B. Jonsson and S. T. Eng, IEEE J. Quantum Electron. **QE-26**, 2025 (1990).

[51] If the δ layers are arranged periodically in a host SL, R of Eq. (3) still bears the meaning of the "concentration" of δ layers, and $R \propto L^{-1}$, where L is the (fixed) distance between the δ layers.

[52] S.-H. Wei and A. Zunger, J. Appl. Phys. **63**, 5794 (1988).

[53] D. M. Bylander and L. Kleinman, Phys. Rev. B**34**, 5280 (1986).

[54] W. Ge, W. D. Schmidt, M. D. Sturge, L. N. Pfeiffer, and K. W. West, J. Lumin. **59**, 163 (1994).

[55] For $n=5$ and $n=6$ we find that the lowest conduction state at $\bar{Z}$ is ≤ 10 meV lower than $\Gamma(X_z)$, making these SLs indirect-gap materials (see Table III in Ref. 48); however, this energy difference is too small to allow a conclusive prediction on the pseudodirect/indirect nature of the band gap.

[58] S. B. Zhang, M. L. Cohen, S. G. Louie, D. Tomanek, and M. S. Hybertsen,

R. A. Mäder and A. Zunger, Appl. Phys. Lett. **64**, 2882 (1994).

[60] Z. Ikonic, G. P. Srivastava, and J. C. Inkson, Phys. Rev. B **46**, 15 150 (1992).

[61] R. Cingolani, L. Tapfer, and K. Ploog, Appl. Phys. Lett. **56**, 1233 (1990).

[62] See, for example, G. Baym, *Lectures on Quantum Mechanics*, 9th ed.

[63] K. A. Mäder and A. Baldereschi, Mater. Res. Soc. Symp. Proc. **240**, 507

[65] M. Kasu, T. Yamamoto, S. Noda, and A. Sasaki, Jpn. J. Appl. Phys. **29**,

for our computational unit cell as was used for the MBE growth of the po-SL.

[67] This discrepancy can be traced back to the EMA error in the $(GaAs)_n(AlAs)_n$, o-SL of $n \sim 1$, 2 in Fig. 7. Around $n \sim 1$, 2, the EMA $\bar{\Gamma}_c(\Gamma)$ (001) states have much larger energies than their EPM counterparts. Apparently, this difference retains in the d-SL.